Received: 31 January 2023 | Revised: 4 May 2023 | Accepted: 6 May 2023

DOI: 10.1002/bit.28434

ARTICLE

BIOTECHNOLOGY AND BIOENGINEERING WILEY

Predictive scaling of fiber-based protein A capture chromatography using mechanistic modeling

Tobias Hahn[1] | Tatjana Trunzer[1] | Florence Rusly[2] | Ryan Zolyomi[2] | Lalita K. Shekhawat[3] | Gunnar Malmquist[3] | Ashley Hesslein[2] | Hendri Tjandra[2]

[1]Cytiva, Karlsruhe, Germany

[2]Bayer, Berkeley, California, USA

[3]Cytiva, Uppsala, Sweden

Correspondence
Tobias Hahn, Cytiva, Global Life Sciences Solutions Germany GmbH, Kriegsstraße 240, Karlsruhe 76135, Germany.
Email: tobias.hahn@cytiva.com

Abstract

Protein A affinity chromatography is an important step in the purification of monoclonal antibodies (mAbs) and mAb-derived biotherapeutics. While the biopharma industry has extensive expertise in the operation of protein A chromatography, the mechanistic understanding of the adsorption/desorption processes is still limited, and scaling up and scaling down can be challenging because of complex mass transfer effects in bead-based resins. In convective media, such as fiber-based technologies, complex mass transfer effects such as film and pore diffusions do not occur which facilitates the study of the adsorption phenomena in more detail and simplifies the process scale-up. In the present study, the experimentation with small-scale fiber-based protein A affinity adsorber units using different flow rates forms the basis for modeling of mAb adsorption and elution behavior. The modeling approach combines aspects of both stoichiometric and colloidal adsorption models, and an empirical part for the pH. With this type of model, it was possible to describe the experimental chromatograms on a small scale very well. An in silico scale-up could be carried out solely with the help of system and device characterization without feedstock. The adsorption model could be transferred without adaption. Although only a limited number of runs were used for modeling, the predictions of up to 37 times larger units were accurate.

KEYWORDS

colloidal particle adsorption model, flow rate dependency, modeling, protein A fibro chromatography, scale-up

1 | INTRODUCTION

Protein A affinity chromatography is an important step in the purification of monoclonal antibodies (mAbs) and mAb-derived biotherapeutics. The purification sequence of mAbs typically starts with protein A capture chromatography and continues with one to three polishing steps using other modes of chromatography (Kelley et al., 2008). Though protein A chromatography resins are expensive and have shorter lifetime in comparison to polishing resins (Ramos-de-la-Peña et al., 2019), it remains an integral part of antibody purification platforms (Liu et al., 2010). Because of its high selectivity and capacity, the achievable purity and yield are typically higher than

95% for mAbs and thereby reduce the separation challenges for the following polishing steps significantly (Shukla et al., 2007).

Protein A is a polypeptide originating from *Staphylococcus aureus* (Hjelm et al., 1972) and thus different compared to the small chemical ligands used for ion-exchange (IEX) or hydrophobic interaction chromatography (HIC). While a mAb is assumed to bind to several of such small ligands at once during IEX or HIC (Mollerup, 2006, 2008), it is the opposite for protein A: Because of its size and constitution, it is assumed that several mAbs can bind to a single protein A ligand (Ghose et al., 2007). Depending on the ligand density and the structure of the base matrix, very different binding and elution behaviors can be observed, which has been the subject of various studies (Hahn et al., 2003, 2005; Pabst et al., 2018). The PrismA ligand used here is a hexamer of an alkaline stabilized Z domain. This suggests that up to at least three mAbs could bind to the same ligand depending on experimental conditions.

While the biopharma industry has extensive expertise in the operation of protein A chromatography, the mechanistic understanding of the adsorption/desorption processes is still limited and thereby its scaling up or scaling down can be challenging (Dimartino et al., 2011; Lienqueo et al., 2011; Montes Sanchez et al., 2004; Tejeda-Mansir et al., 2001). Benner et al. (2019) describe mass transfer effects in bead-based resins as one difficulty for the latter: This has also been a focus of research for Pabst et al. (2018), who found that smaller bead sizes reduce mass transfer limitations, or Reck et al. (2015), who visualized that pore diffusion depends on protein size and loading conditions as well as salt concentration.

In convective media, such as the fiber-based Fibro technology (Figure 1), complex mass transfer effects such as film and pore diffusion do not occur which facilitates studying adsorption effects in more detail and simplifies the process scale-up. However, it must be pointed out that all convective media have an individual topology and thus a distinct flow behavior (Podgornik, 2022). Fibrous adsorbers can be created from various materials, including natural and synthetic polymers, and arranged in different ways for the use as chromatography media. Fiber structures include randomly packed short fibers (Gavara et al., 2012; King & Pinto, 1992; Singh & Pinto, 1995), aligned fibers (Czok & Guiochon, 1990; Marcus et al., 2003) woven fabrics (Yang et al., 1992), and electrospun fiber mats (Hardick et al., 2012) as used in this study. The potential of these materials to increase productivity have been the subject of experimental studies in batch (Gavara et al., 2012, 2015; Hardick et al., 2012) and continuous mode (Hardick et al., 2015), as well as studies employing mechanistic modeling (Winderl et al., 2016).

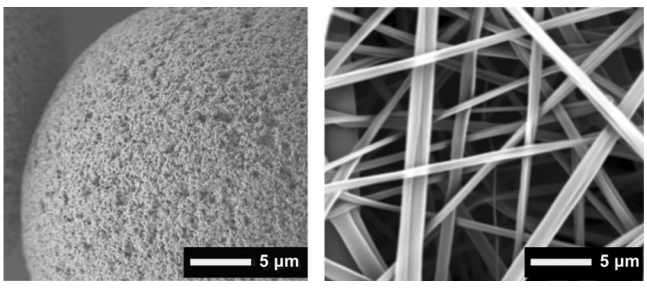

FIGURE 1 Fiber-based chromatography uses a well-defined matrix of cellulose fibers (right) that has a very open structure relative to chromatography beads (left). While beads have a surface area of ~40 m^2/g, most binding sites are only accessible by diffusion. In contrast, the surface area of Fibro of ~10 m^2/g is accessible by convection. The surface area was provided by Cytiva and determined with BET (Brunauer–Emmett–Teller) analysis.

The binding behavior of mAbs to protein A has been described with Langmuir-type isotherms in the past (Lane, 2018; Pabst et al., 2018), while acknowledging that the fundamental assumption of a one-to-one binding mechanism does not hold for protein A chromatography. The more recent modeling approach of Lane (Lane, 2018) also takes the protonation state of both the target mAb and the protein A ligand into account.

The modeling approach employed in this work combines aspects of both stoichiometric and colloidal models. The surface blocking function from the colloidal particle adsorption (CPA) model (Briskot, Hahn, Huuk, & Hubbuch, 2021; Briskot, Hahn, Huuk, Wang, et al., 2021) was used in combination with a pH-dependent equilibrium coefficient and a finite rate of adsorption kinetics, as first used by Thomas for nonporous particles (Thomas, 1944). The derivation of the surface saturation function is independent of the chromatography mode and is thus assumed to be transferrable to affinity chromatography.

When modeling membranes, monoliths, and fiber-based materials, precise system and device characterization is of great importance as hold-up volumes in the devices can exceed the functionalized adsorber volume. In this study, extensive experimentation at different flow rates with tracer substances were performed for three system scales, with and without prototypical Fibro units with volumes ranging from 4.3 to 160 mL. The Fibro units consist of the PrismA affinity ligand coupled to electrospun cellulose nanofiber adsorbents. Following the fundamental assumption of *in silico* scale-up and scale-down of chromatography, that the adsorption model is scale-independent, four bind-and-elute experiments at 4.3 mL small scale were needed to calibrate the model. The model is then used to predict the behavior of 40 and 160 mL Fibro prototype units.

2 | THEORY

2.1 | Adsorption model

Sandoval et al. (2012) developed a model for affinity chromatography by following a common stoichiometric approach and adding a pH-relationship empirically. Here, one mole of protein molecule P in solution is assumed to bind to one mole of protein A ligands L, forming one mole of protein-ligand complexes PL:

$$P + L \rightleftharpoons PL. \quad (1)$$

Theoretically, it would be possible to extend the above equation with a stoichiometric coefficient to describe that three mAbs can bind to one PrismA ligand. However, as it is unclear whether the full saturation happens also under all conditions, Equation (1) was used unmodified. Applying the law of mass action, the equilibrium formulation was derived to be

$$\frac{q}{c} = k_{eq}\bar{q}, \tag{2}$$

where c and q are the molar protein concentrations in solution and bound to the stationary phase, respectively. $\bar{q}$ is the normalized concentration of available ligands which is later replaced by the CPA surface coverage function, as also applied in Hahn et al. (2022).

Similar to Hunt et al. (2017) for IEC and Hahn et al. (2018) for HIC, the pH-dependency of the equilibrium constant, k_{eq} was empirically included by Sandoval et al. (2012) as

$$k_{eq}(pH) = k_{eq0}\cdot 10^{k_{eq1}\cdot(pH-pH_{ref})}. \tag{3}$$

In this work, we added a second order term to achieve a better agreement with the experimental data, and also included an exponential influence of the salt concentration times the interaction parameter K_s, stemming from Mollerup's model of the protein solute activity coefficient (Mollerup, 2008):

$$k_{eq}(pH) = k_{eq0}\cdot 10^{k_{eq1}\cdot(pH-pH_{ref})+k_{eq2}\cdot(pH-pH_{ref})^2}\cdot \exp^{K_S\cdot c_{salt}}. \tag{4}$$

As later shown in Table 4, the second order term limits the k_{eq} value at binding pH and allows for a steep slope at the point of elution. This is especially beneficial when simulating long gradient elutions. Adding the K_s term to a protein A model was first proposed in Schwan (2019).

The general structure of the nonlinear isotherm follows the CPA formalism for ion-exchange chromatography (Briskot, Hahn, Huuk, & Hubbuch, 2021). The rate of change of the bound protein concentration is described by a constant kinetic rate k_{kin} and adsorption and desorption terms, multiplied by the protein concentrations in solution and adsorbed state, respectively.

$$\frac{\partial q}{\partial t} = k_{kin}[k_{eq}(pH)\cdot B(A_s, a)\cdot c - q]. \tag{5}$$

The available surface function B from the CPA model depends on the resin specific surface area A_s, a material-specific constant, and protein colloid radius a. It is explained in detail in Briskot, Hahn, Huuk, Wang, et al. (2021).

A summary of all model parameters and their physical meaning is given in Table 1.

2.2 | Column model

In the absence of microporous volumes that are accessible by diffusion only, a lumped kinetic model (Seidel-Morgenstern, 2020) was selected to describe the temporal change of the solute bulk concentration c_i of solute i:

$$\frac{\partial c_i}{\partial t}(x,t) = -\ u_{int}\frac{\partial c_i}{\partial x}(x,t) + D_{app,i}\frac{\partial^2 c_i}{\partial x^2}(x,t) - \frac{1-\varepsilon_t}{\varepsilon_t}\frac{\partial q_i}{\partial t}(x,t), \tag{6}$$

where x represents the axial position within the column, t is the time, D_{app} denotes the apparent dispersion coefficient, u_{int} is the interstitial velocity, ε_t represents the void fraction, and q_i represents the concentration of the i-th solute with respect to the adsorber skeleton volume.

The column model is complemented with Danckwerts boundary conditions

$$\frac{\partial c_i}{\partial x}(0,t) = \frac{u_{int}}{D_{app,i}}(c_i(0,t) - c_{in,i}(t)), \tag{7}$$

$$\frac{\partial c_i}{\partial x}(L,t) = 0, \tag{8}$$

where $c_{in,i}$ is the prescribed concentration of species i at the inlet of the column.

3 | MATERIALS AND METHODS

3.1 | Chromatographic instrumentation

The prototypical Fibro units with PrismA protein A ligands used in this study covered laboratory to pilot scale, ranging from matrix

TABLE 1 Summary of component-specific adsorption model parameters.

Model parameter	Unit	Meaning
Protein radius a_i	[m]	A protein is represented by a sphere with radius a_i.
Equilibrium coefficient $k_{eq,i}(pH)$	[−]	pH-dependent equilibrium constant derived from the application of the law of mass action.
Kinetic constant $k_{kin,i}$	[s^{-1}]	Measure for the rate of adsorption/desorption.
Specific adsorber surface to volume ratio $A_{s,i}$	[m^{-1}]	Adsorber surface per adsorber skeleton volume accessible by the mAb.
Activity coefficient parameter $K_{s,i}$	[M^{-1}]	Influence of salt concentration on the asymmetric activity coefficient

volumes (or membrane volumes, MV) of 4.3 mL (small scale Fibro PrismA) to 40 mL (medium scale Fibro PrismA), up to 160 mL (pilot scale Fibro PrismA). Experiments were performed on three different chromatography systems: ÄKTA avant 150, ÄKTA pilot 600, and ÄKTA ready with Low Flow Kit (all Cytiva, Little Chalfont), each controlled with the software UNICORN 7.0.2. The systems were chosen fitting to the volumetric flow rate recommended to operate the specific Fibro units. Accordingly, the ÄKTA avant 150 was combined with the 4.3 mL small scale unit, the ÄKTA pilot 600 with the 40 mL medium scale Fibro unit, and the ÄKTA ready with the 160 mL pilot scale Fibro unit. It should be pointed out once again that the units used in this study were prototypes that differ slightly from those commercially available in geometry (compare with HiTrap™ Fibro PrismA and HiScreen™ Fibro PrismA units datafile, 2022). The system characteristics were determined with salt step change experiments, the Fibro unit size measurements and porosity of the functional fiber layer and non-woven layer were determined experimentally. Detailed experiment information can be found in Section 3.3.

3.2 | Buffers and feedstock

System and column-specific effects were determined with a step change experiment in which a 50 mM NaCl equilibration buffer was replaced with a mobile phase with 300 mM NaCl with 1% acetone. To perform mAb capture in pH-controlled bind-and-elute mode, a buffer with 50 mM Tris and 50 mM NaCl at pH 7 was used for equilibration and a first wash phase. A second high-salt wash was performed with a 50 mM acetate buffer with additional 1 M NaCl at pH 5.5. pH step elution started at pH 6 and went down to pH 3.4 using 50 mM acetate buffers containing 50 mM NaCl. In case of linear pH gradient elutions, lower pH ranges were used to ensure complete elutions: The gradients started with a 50 mM acetate buffer containing 30 mM NaCl at pH 5 and ended with a 50 mM acetate buffer containing 50 mM NaCl at pH 3. Sanitization was performed with 0.5 M NaOH.

The antibody feedstock used in this study is derived from industrial CHO cultivation. The clarified cell culture fluid (pH = 7.2, 13 mS/cm) with an antibody titer of 4.7 g/L was filtered before loading and included a monomer species, as well as high molecular weight (HMW) and low molecular weight (LMW) variants, and host cell proteins (HCPs) which were not analyzed further within this case study.

3.3 | Experimental design

The ÄKTA avant 150 and the ÄKTA pilot 600 systems as well as the respective Fibro units (4.3 and 40 mL) were characterized with salt step change experiments at 3.5 and 7 MV/min, and 4 and 8 MV/min, respectively. The ÄKTA ready with the 160 mL Fibro prototype was characterized with a salt step change experiment at 4 MV/min.

To study the adsorption behavior of the mAb, both gradient and step elution experiments were performed at the lab-scale (ÄKTA avant 150 with small scale Fibro PrismA prototype). The pH gradient experiments with different gradient slopes were performed at 3.5 MV/min, a similar experiment with partial breakthrough was performed with flow rates of 3.5 and 7 MV/min. The experiments performed at gradient lengths of 21.5 and 34.4 MV are designed to determine the change of elution pH as a function of gradient slope, similar to the experimental design used for Yamamoto method (Yamamoto et al., 1983) but without analytical parameter determination. The pH step elution experiment was performed at 3.5 MV/min at small scale and 4 MV/min on the other scales. The lab-scale experiment was used for model calibration, and the ones on the two larger scales for model validation. Moreover, a pH step elution experiment was performed at twice the original flow rate to validate the model at laboratory and medium scale. All step elution experiments at medium and pilot scale followed the same approach: after equilibration for 5 MV, the Fibro units were loaded with 28–30 g/L_{MV}, followed by low salt and high salt washes of 9 MV. The step elution lasted for 6 MV, and the sanitization 4 MV. Subsequent to this, the system was re-equilibrated for 7 MV. The small scale step experiment used the same sequence of phases but each duration in MV was chosen 14% shorter.

An overview of the performed scale-dependent system and column characterization experiments, as well as model calibration and validation experiments can be found in Table 2.

3.4 | Numerical methods

The simulations were performed using the GoSilico Chromatography Modeling Software version 1.12.0, which is based on ChromX (Hahn et al., 2015). A finite element method with linear elements was used together with discretization in time using the Fractional step θ time-stepping algorithm (Hindmarsh et al., 2005).

3.5 | Model parameter estimation and model-based scale-up

The systems and Fibro units were modeled using dispersed plug flow reactors (DPFRs) and continuously stirred tank reactors (CSTRs). Model parameters were estimated from the salt step change experiments. The flow rate dependent CSTR and DPFR effects are system/unit specific and were kept constant when continuing model calibration with bind-elute experiments.

The adsorption parameter estimation was performed sequentially using the experimental results obtained on small scale Fibro unit. pH was simulated as a mobile phase modifier according to Equation 6). All parameters of the equilibrium adsorption isotherm were expected to be scale- and flow-independent and estimated simultaneously. The initial estimation was performed with an adaptive simulated annealing algorithm (Ingber, 1993) using all four

TABLE 2 Overview of characterization, calibration, and validation experiments.

	Experimental conditions	Flow rate (MV/min)
System characterization		
ÄKTA avant 150	Step change with high salt buffer	3.5, 7
ÄKTA pilot 600		4, 8
ÄKTA ready		4
Fibro unit characterization		
4.3 mL small scale Fibro PrismA prototype	Step change with high salt buffer	3.5, 7
40 mL medium scale Fibro PrismA prototype		4, 8
160 mL pilot scale Fibro PrismA prototype		4
Calibration at lab-scale (ÄKTA avant 150 with small scale Fibro PrismA prototype)		
Linear gradient experiments	22 and 34 MV gradient elution, mAb sample in 100 mM NaCl	3.5
mAb breakthrough	Step elution, mAb sample in 50 mM NaCl	3.5, 7
Step experiment	Step elution, mAb sample in 100 mM NaCl	3.5, 7
Validation by cross-scaling		
ÄKTA pilot 600 with 40 mL Fibro PrismA	Step elution, mAb sample in 100 mM NaCl	4, 8
ÄKTA ready with 160 mL Fibro PrismA		4

lab-scale experiments at a flow rate of 3.5 MV/min and the normalized least squares error norm. Model parameters were finally refined using a Levenberg-Marquardt algorithm (Agarwal & Mierle, 2022).

The model uncertainty was evaluated with forward finite differences to compute the approximate parameter covariance matrix and confidence intervals. After model calibration and quality assessment, the model was used for in silico process scale-up by applying only the scale-specific fluid dynamic parameters and keeping the molecule-specific adsorption parameters determined in small scale constant.

3.6 | Evaluation of flow rate dependent binding kinetics

A detailed analysis of flow rate dependent binding effects was performed independently from the main study and is discussed in Section 4.3. For this, an ÄKTA avant with a HiTrap Fibro PrismA (HiTrap™ Fibro PrismA and HiScreen™ Fibro PrismA units datafile, 2022) unit of 0.4 mL was used. Loading till breakthrough with a second purified industrial mAb, followed by pH step elution was performed at different flow rates ranging from 5 to 40 MV/min. 20 mM phosphate buffer containing 150 mM NaCl (pH 7.4) was used as equilibration and wash buffer (attained after 100% breakthrough when the UV cell was saturated). The pH step elution is induced with 50 mM acetate buffer (pH = 3.5). Afterward, cleaning-in-place is performed with 0.5 M NaOH. The HiTrap unit was loaded with 1 g/L mAb buffer exchanged into 20 mM phosphate buffer (pH = 7.4) containing 150 mM NaCl.

4 | RESULTS AND DISCUSSION

4.1 | System and column characterization

To describe the systems precisely, that is, as individually configured, each ÄKTA system is represented in the model as a composition of system tubing and equipment items such as restrictors (i.e., pump restrictor), valves (i.e., injection valve, column valve) and sensors (i.e., UV cell, conductivity cell) as present and measurable in the real system (ÄKTA avant chromatography system, 2022; ÄKTA pilot 600 chromatography system, 2022; ÄKTA ready and ÄKTA ready XL Flow Kits, 2022). Figure 2 gives an overview of the system configuration with and without a Fibro unit attached. Characterizing these two cases independently allows differentiation between system-specific or Fibro unit-specific fluid dynamic effects. The ÄKTA avant system is modeled starting at the injection valve, and, separately, starting

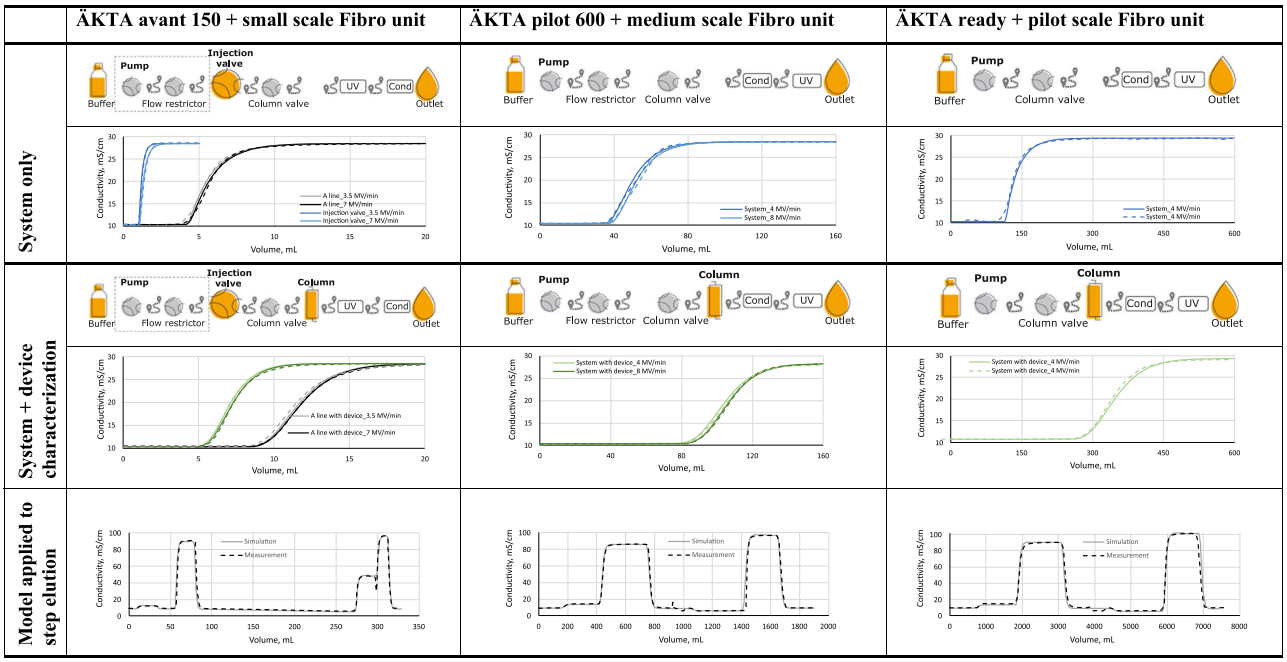

FIGURE 2 System configuration and Fibro PrismA unit characterization. Dashed lines represent the experiment, solid lines the simulation signal of the calibrated model. Lighter colored curves show experiments performed at lower (3.5 or 4 MV/min), darker colored curves the corresponding experiments at higher flow rates (7 or 8 MV/min). The conductivity curves in the bottom row show validation runs based on the system + device model, all at lower flow rate.

TABLE 3 Fibro unit geometries and flow rate-dependent apparent dispersion parameters. More information can be found in the Supporting Information.

Property	Unit	Small scale Fibro unit		Medium scale Fibro unit		Pilot scale Fibro unit
Membrane volume V	[mL]	4.31		40.12		160.48
Functionalized membrane thickness L	[mm]	2.2		2.2		2.2
Total porosity ε_t	[−]	0.676		0.676		0.676
Flow rate	[MV min^{-1}]	3.5	7	4	8	4
	[mm s^{-1}]	0.1283	0.3780	0.1467	0.2933	0.1467
Apparent dispersion $D_{app,salt}$	[mm^{2}s^{-1}]	0.0512	0.1058	0.0252	0.0385	0.0385

from the buffer line. The different results highlight the significant impact of the flow path composition: While the tubing length does not change enough to affect the band broadening, the retention time and mixing effects increase when the sample is not directly injected at the injection valve but applied via the buffer line (pump wash included). This is due to additional equipment items such as pump restrictor or mixer valve.

The chromatograms in Figure 2 visualize the calibrated system models, in which the measured, dashed curves fit the simulated, solid conductivity traces well. The larger the applied flow rate, the more significant is the dispersion in the tubing and the Fibro unit (see Supporting Information and Table 3). Both the tubing as well as devices installed are system and scale specific. Therewith, the determined tubing dispersion coefficient (depending on tubing diameter and length) as well as the devices' mixing effects and delays (depending on void volume) cannot be compared directly to each other. However, it is safe to assume that the axial dispersion coefficient of the tubing decreases for increasing tubing diameter, while the device mixing effects increase with increasing void volume. The determined Fibro units' apparent dispersion coefficients depends on the device design. In this regard, the small prototype deviates from the two larger ones as it is constructed differently. However, the design is similar for the medium and pilot scale units as the internal void volume increases for the large Fibro unit but not the dispersion effects for the membrane itself. All considered measured or

estimated parameters are listed in detail in the Supporting Information.

After finalizing the fluid dynamic model at all scales, it was validated with three exemplary experiments from the calibration set, illustrated in the bottom row of Figure 2 (experiments performed at low flow rate, 3.5 MV for ÄKTA avant and 4 MV/min for ÄKTA pilot and ready). The measured conductivity is well described by the simulation. This shows that the simple salt step change experiments are sufficient for calibration and the resulting model with flow rate-dependent dispersion parameters is applicable to more complex chromatography methods with differently concentrated buffer solutions.

4.2 | Model calibration with bind-and-elute experiments

To describe the mAb-protein A ligand interaction, the newly developed affinity isotherm was calibrated by curve fitting. The resulting parameters are listed in Table 4. Assuming that neither the equilibrium coefficient nor the blocking function (see Equation 5) is flow-dependent (assumption discussed in detail in Section 4.3), the model is calibrated based on two low-loaded gradient experiments, one partial breakthrough and one step experiment performed at 3.5 MV/min at lab-scale. The simulated chromatograms are shown in Figure 3 together with the respective measured UV signals. The breakthrough profile was simulated with a nonbinding species with the inlet concentration adjusted to match the observed UV level. Further, to account for UV detector saturation, the simulated UV traces were limited to 3000 mAU. The curves agree well, and model quality was assessed with the help of calculated approximate confidence intervals. Subsequently, using a step elution at a flow rate of 7 MV/min, the apparent dispersion coefficient for the mAb was estimated again with unchanged isotherm parameters. The determined 95% confidence intervals for the adsorption model are small and indicate that a change of parameters values has an impact on the goodness of fit (see Table 4). An exception is the large confidence interval of the K_s parameter, which means that the influence of the salt concentration changes is not well quantifiable from the set of calibration experiments. As the process is pH-driven, this remaining uncertainty was considered acceptable. The estimated specific surface area is smaller than that for the bead-based resin Capto S ImpAct by a factor of 8–9 (Briskot, Hahn, Huuk, Wang, et al., 2021) which fits well to the ratio of surface area per gram given in Figure 1. In comparison to a packed column, the apparent dispersion parameter value is slightly larger for the lab-scale setup, but still in the same order of magnitude (0.32–0.78 mm²/s for Capto S ImpAct [Briskot, Hahn, Huuk, Wang, et al., 2021]), despite the significantly higher flow rates. The differences in the values for the two flow rates of 3.5 and 7 MV/min are not significant, especially considering the confidence intervals. The comparably large confidence interval indicates that it is not well determinable from these bind-and-elute experiments. Additional experiments under nonbinding conditions could reduce the uncertainty.

By plotting the log k_{eq} term from Equation (2) over pH as shown in Table 4, strong adsorption of the mAb species is

TABLE 4 Calibrated model parameters. The approximate 95% confidence interval expressed as a percentage of the parameter value is given in brackets.

Parameter	Unit	ÄKTA avant 150	ÄKTA pilot 600	ÄKTA ready
A_s	[m^{-1}]	8.22e + 07 (±0.07%)		
$D_{app,mAb}$ at low flow rate	[mm^2s^{-1}]	1.4698 (± 17.4%)	0.2449	0.2449
$D_{app,mAb}$ at high flow rate	[mm^2s^{-1}]	1.0937 (± 37.0%)	0.1133	n.a.
Porosity	[%]	67.6		
a	[m]	5.5×10^{-9}		
k_{eq0}	[−]	7944.74 (±2.11%)		
k_{eq1}	[pH^{-1}]	5.5214 (±2.94%)		
k_{eq2}	[pH^{-2}]	−1.8564 (±3.18%)		
k_{kin}	[s^{-1}]	0.2743 (±4.98%)		
K_S	[M^{-1}]	−1.185 (±25.40%)		

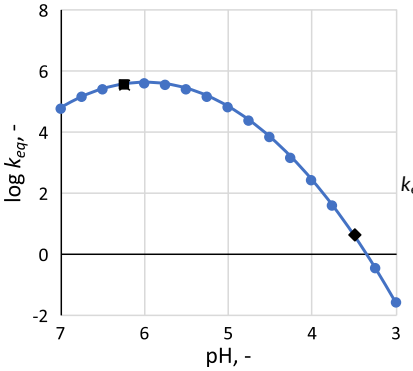

k_{eq} plot of CPA parameters. The square and circle markers indicate the pH value of the loading buffer and elution buffer, respectively.

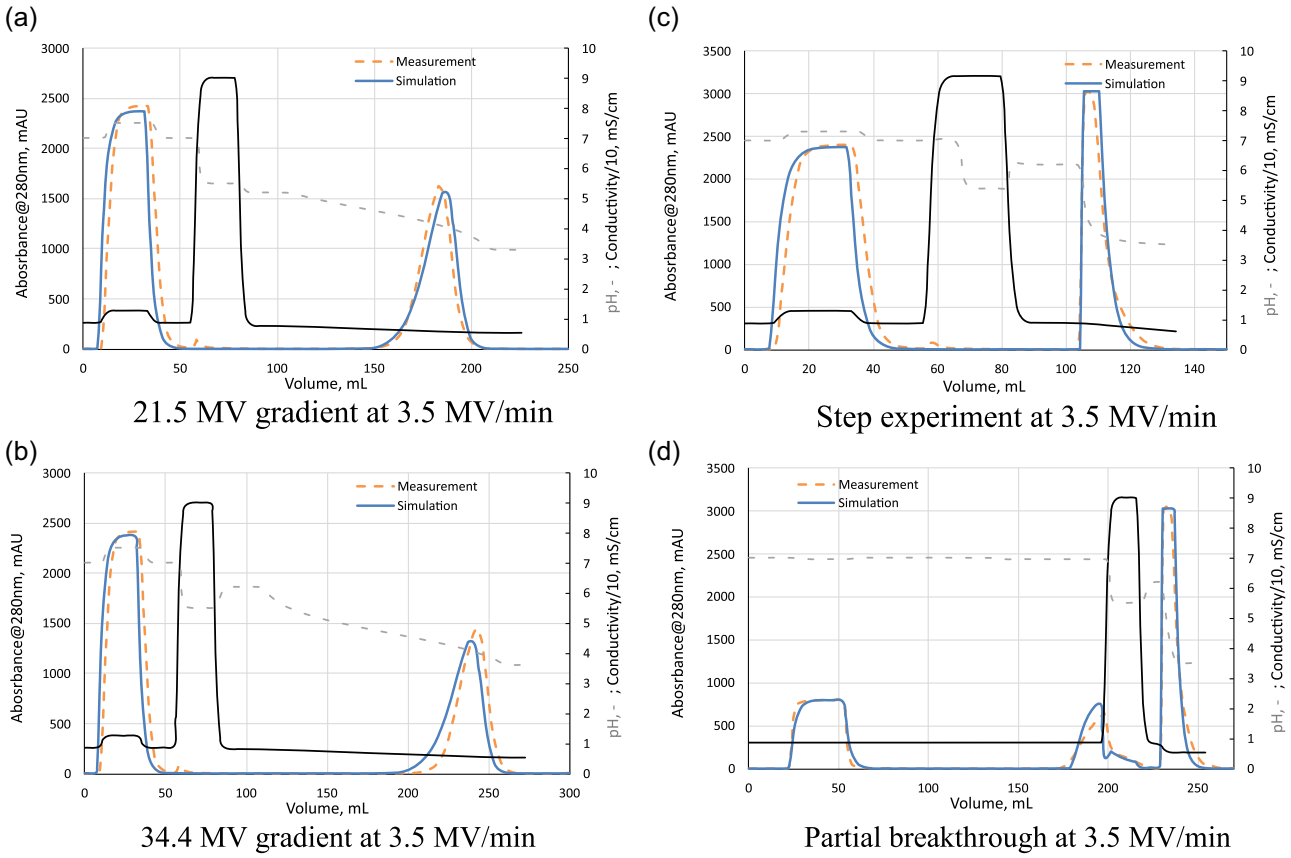

FIGURE 3 Model calibration on ÄKTA avant 150 with small scale Fibro PrismA. The orange, dashed line represents the experimental results, the blue, solid line the simulated UV curve. The grey, dash-dotted line represents the pH, the conductivity signal is printed in black.

confirmed for the loading buffer conditions at pH 6.2. Desorption conditions are present when injecting the elution buffer (pH 3.5), as log k_{eq} becomes smaller than 1. For comparison, the log k_{eq} value reported in Lane (2018) for a different mAb and adsorber combination at pH 7 was 3–4 which is similar to the magnitude reported here. The inverse value of k_{kin}, which is approximately 3.65, is within in the range of 0.75–10 reported for IgG's in Sandoval et al. (2012); and the slightly negative K_s value is in the same order of magnitude as observed for the pH-controlled mixed-mode process in Hahn et al. (2022).

4.3 | Influence of flow rate on mAb-Fibro interactions

To investigate the influence of the flow rate on adsorption/desorption processes in detail, experiments with various flow rates were performed with a HiTrap Fibro unit, which was overloaded with a second mAb (exemplary breakthrough curves are illustrated in Figure 4a, left) and eluted with a pH step (see Figure 4a, right). The mAb breakthrough curves indicate that the attainable dynamic binding capacity at 50% breakthrough increases slightly with decreasing flow rate.

This might be caused by the probability of mAb/ligand interaction increasing the slower the flow conditions are. Besides, some binding sites might be more likely reachable by diffusion, even when this is not a substantial factor in this convection-dominated system. For flow rates faster than 10 MV/min, the observed behavior did not change further in this study. The breakthrough curves overlap and indicate no further reduction in accessibility of binding sites or unfavorable binding kinetics. From a modeling perspective, neither the equilibrium term nor the blocking function of the chosen model can be flow dependent by definition. The kinetic constant might be considered flow-dependent such that a higher flow rate decreases the (re-) binding likelihood. However, the desorption rate seems unaffected as the elution peak tailing is similar for different flow rates. Thus, to describe the observed behavior under slower flow, a major rework of the model structure is needed, as well as more precise experimental data, which are beyond the scope of this study.

Transferring these findings to the main case study, it was to be expected that an increase of the flow rate from 4 to 8 MV/min would

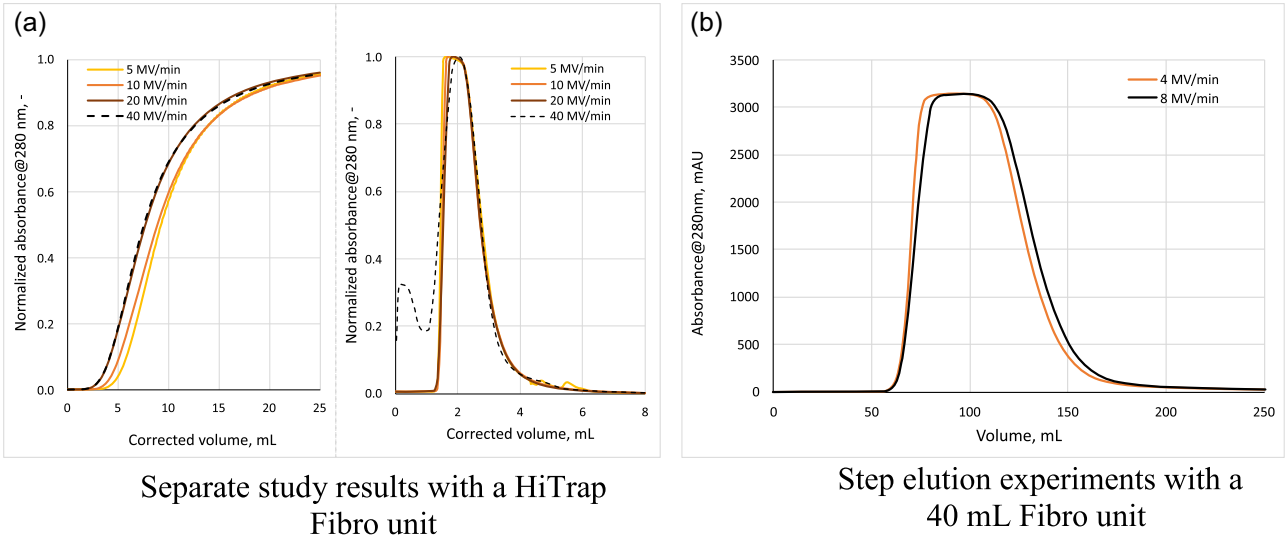

FIGURE 4 Two studies of flow rate dependent adsorption/desorption effects. (a) The presented experiments were performed with a second mAb species on an ÄKTA avant with HiTrap Fibro PrismA. Left: breakthrough curves at different flow rates. Right: pH-step induced elution. (b) The presented experimental curves show an overlay of the elution peaks at 4 and 8 MV/min performed on ÄKTA pilot 600 with 40 mL Fibro prototype. For better visualization, the *x*-axis begins with the respective starting point of the individual process step, that is, the loading phase or elution phase.

have little influence on the elution peak shape of the mAb capture step experiments. The result of such an experiment with the ÄKTA pilot 600 and the 40 mL Fibro unit is shown in Figure 4b. The elution peak shapes are similarly curved as hypothesized, therewith confirming the observations made with the HiTrap unit. Thus, adsorption model parameter determination can be done at a constant flow rate with low risk of loss of predictive power as long as the unit is not overloaded.

4.4 | Model validation and scale-up

The model validity for an elevated flow rate of 7 MV/min at lab-scale was evaluated with a partial breakthrough and a step elution experiment illustrated in Figure 5a. As expected, no significant change in peak shape in either the model or the experimental data occurred. The goodness of fit for the breakthrough and elution peak is the same as for the low flow rate.

Next, the standard step elution experiment was scaled up in silico. Initially, the same ratio of $D_{app,salt}$ to $D_{app,mAb}$ as observed for the lab-scale system was used to predict the outcome of the step elution experiment on the ÄKTA pilot system with 40 mL Fibro unit. However, the calculated $D_{app,mAb} = 0.72\ mm^2/s$ lead to an increased peak tailing compared to the experimental chromatogram (data not shown). A re-estimation of the $D_{app,mAb}$ parameter for the pilot Fibro unit for both flow rates lead to the values given in Table 4. $D_{app,mAb}$ was found to be 10 times larger then $D_{app,salt}$ but not 30 times larger as for the lab-scale unit. One possible cause could be that D_{app} does not only model the dispersive effects along the functionalized membrane, but also the back mixing at the inlet according to Equation (7). The fact that the flow path is split for the lab-scale prototype (c.f (HiTrap™ Fibro PrismA and HiScreen™ Fibro PrismA units datafile, 2022)) but not for the other scales may account for differences in mixing behavior. In contrast, the further scale-up from 40 to 160 mL worked as expected with the same newly determined $D_{app,mAb} = 0.24\ mm^2/s$ value at 4 MV/min.

The resulting chromatograms for the ÄKTA pilot system with the 40 mL Fibro unit and two different flow rates are shown in Figure 5b and for the ÄKTA ready system with 160 mL Fibro unit for 4 MV/min in Figure 5c. The simulated curves result from using the system-specific fluid dynamic model (Figure 2) together with the determined adsorption model parameters from Section 4.2.

All runs show very good agreement with the simulated curves. This confirms that accurate scale-up predictions are possible if the model is calibrated with few a laboratory-scale experiments and if the differences in system configuration and fluid dynamics are taken into account. The protein-ligand interactions can be assumed to be scale-invariant.

As shown in Table 5, the measured and predicted elution pool volume and mAb yield are overall, in good agreement. The reduced yield of the pilot scale experiment is likely caused by the visible breakthrough at the end of the load phase which was not predicted by the simulation. Overall, the consistently high yields and fast processing times show that Fibro units are a potential alternative to standard bead-based protein A resins.

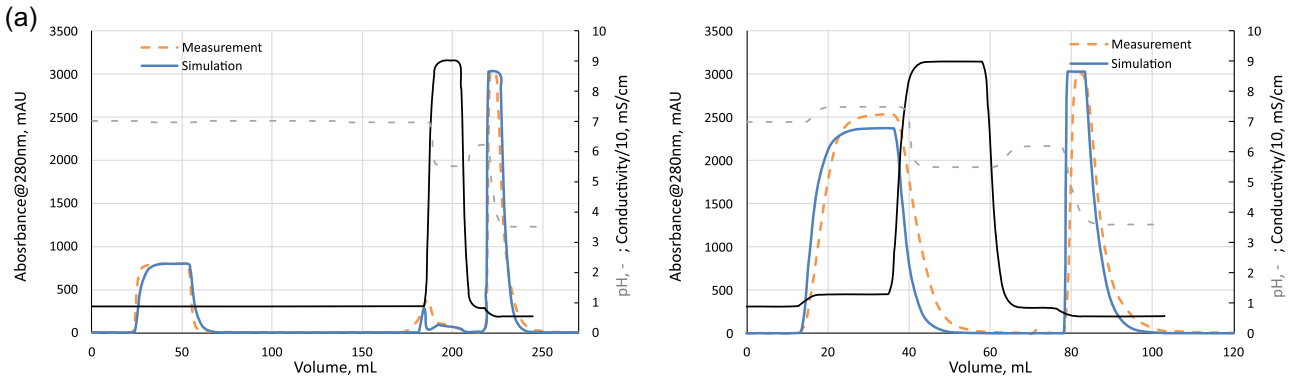

Laboratory scale: Partial breakthrough experiment (left) and step elution (right) at 7 MV/min on ÄKTA avant with 4.3 mL small scale Fibro unit

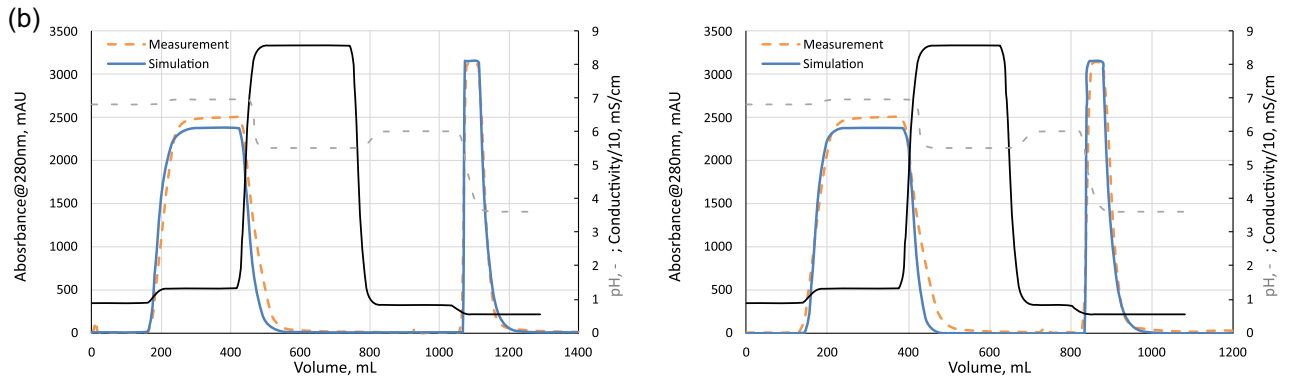

Medium scale: Step experiments at 4 MV/min (left) and 8 MV/min (right) on ÄKTA pilot 600 with 40 mL Fibro unit

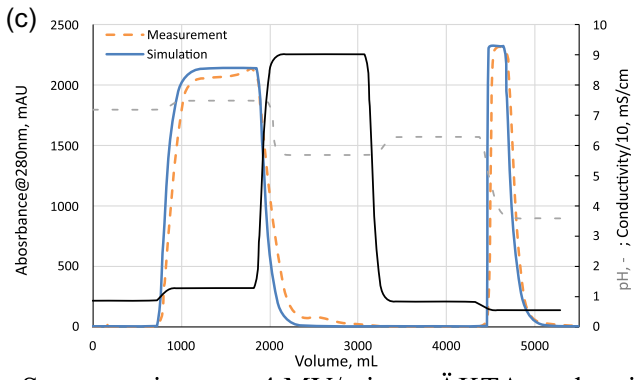

Pilot scale: Step experiment at 4 MV/min on ÄKTA ready with 160 mL Fibro unit

FIGURE 5 Validation experiments at different scales. The orange, dashed line represents the experimental chromatogram; the blue, solid line the simulated UV curve. pH is shown as dash-dotted line in grey, the conductivity signal as solid line in black.

TABLE 5 Comparison of mAb fraction yield predicted by simulation and validated experimentally for the step experiments at 3.5 or 4 MV/min at different scales.

Scale	Experimental results		Simulation predictions	
	Fraction volume (MV)	Yield (%)	Fraction volume (MV)	Yield (%)
ÄKTA avant with small scale Fibro unit	5.3	97.8	5.6	99.9
ÄKTA pilot with 40 mL Fibro unit	3.0	97.4	3.0	98.8
ÄKTA ready with 160 mL Fibro unit	3.5	94.5	3.2	99.2

5 | CONCLUSIONS

In this study, we examined three different sized Fibro PrismA prototypes experimentally and simulatively. To be able to distinguish precisely between scale-independent thermodynamics and scale-dependent fluid dynamics, a thorough system characterization with pulse experiments with and without a Fibro unit inline was carried out for each scale. The thermodynamic model was then only calibrated on laboratory scale. To describe the affinity chromatography, the surface coverage function from the colloidal particle adsorption model was used in combination with a pH-dependent stoichiometric model and a finite rate of adsorption kinetics. Separating the flow rate-dependent system and device characteristics from the mAb adsorption, the lab-scale-calibrated model could be applied successfully to predict elevated flow rates as well as the behavior of the 9- to 37-fold larger medium-scale and pilot-scale prototypes. As only four experiments with mAb feedstock were used for model calibration, the presented method allows rapid development of fiber-based protein A processes with limited material expenditure, and subsequent scale-up using only few pulse experiments for system characterization.

ACKNOWLEDGMENTS

The authors thank Till Briskot, who developed the type of adsorption models used in Hahn et al. (2022), as well as this study, and thus created an essential basis for this work.

CONFLICTS OF INTEREST STATEMENT

The authors affiliated to Cytiva declare, that the HiTrap Fibro PrismA unit, the ÄKTA systems, as well as the software packages UNICORN and GoSilico Chromatography Modeling Software used in the manuscript are commercial products from Cytiva.

DATA AVAILABILITY STATEMENT

Research data are not shared.

ORCID

Tobias Hahn http://orcid.org/0000-0001-7030-2037
Tatjana Trunzer https://orcid.org/0000-0003-4444-0860

REFERENCES

Agarwal, S., & Mierle, K. (2022). *Ceres solver*. The Ceres Solver Team. https://github.com/ceres-solver/ceres-solver

ÄKTA Avant Chromatography System. https://www.cytivalifesciences.com/en/us/shop/chromatography/chromatography-systems/akta-avant-p-06264

ÄKTA Pilot 600 Chromatography System. https://www.cytivalifesciences.com/en/us/solutions/bioprocessing/products-and-solutions/downstream-bioprocessing/akta-pilot-600

ÄKTA Ready and ÄKTA Ready XL Flow Kits. https://www.cytivalifesciences.com/en/us/shop/chromatography/chromatography-flow-kits/akta-ready-flow-kits-p-04247

Benner, S. W., Welsh, J. P., Rauscher, M. A., & Pollard, J. M. (2019). Prediction of lab and manufacturing scale chromatography performance using mini-columns and mechanistic modeling. *Journal of Chromatography A*, *1593*, 54–62. https://doi.org/10.1016/j.chroma.2019.01.063

Briskot, T., Hahn, T., Huuk, T., & Hubbuch, J. (2021). Protein adsorption on ion exchange adsorbers: A comparison of a stoichiometric and non-stoichiometric modeling approach. *Journal of Chromatography A*, *1653*, 462397. https://doi.org/10.1016/j.chroma.2021.462397

Briskot, T., Hahn, T., Huuk, T., Wang, G., Kluters, S., Studts, J., Wittkopp, F., Winderl, J., Schwan, P., Hagemann, I., Kaiser, K., Trapp, A., Stamm, S. M., Koehn, J., Malmquist, G., & Hubbuch, J. (2021). Analysis of complex protein elution behavior in preparative ion exchange processes using a colloidal particle adsorption model. *Journal of Chromatography A*, *1654*, 462439. https://doi.org/10.1016/j.chroma.2021.462439

Czok, M., & Guiochon, G. (1990). Aligned fiber columns for size-exclusion chromatography. *Journal of Chromatography A*, *506*, 303–317. https://doi.org/10.1016/s0021-9673(01)91586-9

Dimartino, S., Boi, C., & Sarti, G. C. (2011). Influence of protein adsorption kinetics on breakthrough broadening in membrane affinity chromatography. *Journal of Chromatography A*, *1218*(26), 3966–3972. https://doi.org/10.1016/j.chroma.2011.04.062

Gavara, P., Bibi, N., Sanchez, M., Grasselli, M., & Fernandez-Lahore, M. (2015). Chromatographic characterization and process performance of column-packed anion exchange fibrous adsorbents for high throughput and high capacity bioseparations. *Processes*, *3*(1), 204–221. https://doi.org/10.3390/pr3010204

Gavara, P. R., Cabrera, R., Vennapusa, R. R., Grasselli, M., & Fernandez-Lahore, M. (2012). Preparation, characterization, and process performance of composite fibrous adsorbents as cation exchangers for high throughput and high capacity bioseparations. *Journal of Chromatography B*, *903*, 14–22. https://doi.org/10.1016/j.jchromb.2012.06.027

Ghose, S., Hubbard, B., & Cramer, S. M. (2007). Binding capacity differences for antibodies and Fc-fusion proteins on protein A chromatographic materials. *Biotechnology and Bioengineering*, *96*(4), 768–779. https://doi.org/10.1002/bit.21044

Hahn, R., Bauerhansl, P., Shimahara, K., Wizniewski, C., Tscheliessnig, A., & Jungbauer, A. (2005). Comparison of protein A affinity sorbents. *Journal of Chromatography A*, *1093*(1–2), 98–110. https://doi.org/10.1016/j.chroma.2005.07.050

Hahn, R., Schlegel, R., & Jungbauer, A. (2003). Comparison of protein A affinity sorbents. *Journal of Chromatography B*, *790*(1–2), 35–51. https://doi.org/10.1016/s1570-0232(03)00092-8

Hahn, T., Geng, N., Petrushevska-Seebach, K., Dolan, M. E., Scheindel, M., Graf, P., Takenaka, K., Izumida, K., Li, L., Ma, Z., & Schuelke, N. (2023). Mechanistic modeling, simulation, and optimization of mixed-mode chromatography for an antibody polishing step. *Biotechnology Progress*, *39*, 3316. https://doi.org/10.1002/btpr.3316

Hahn, T., Huuk, T., Heuveline, V., & Hubbuch, J. (2015). Simulating and optimizing preparative protein chromatography with ChromX. *Journal of Chemical Education*, *92*(9), 1497–1502. https://doi.org/10.1021/ed500854a

Hahn, T., Wang, G., Läufer, T., Vasalas Peralvarez, M., Huuk, T., & Hubbuch, J., (2018). *Mechanistic extension of a hydrophobic interaction chromatography model to account for pH changes and mixed-mode binding*. Presented at Recovery of Biological Products XVIII, October 8, 2018.

Hardick, O., Dods, S., Stevens, B., & Bracewell, D. G. (2012). Nanofiber adsorbents for high productivity downstream processing. *Biotechnology and Bioengineering*, *110*(4), 1119–1128. https://doi.org/10.1002/bit.24765

Hardick, O., Dods, S., Stevens, B., & Bracewell, D. G. (2015). Nanofiber adsorbents for high productivity continuous downstream processing. *Journal of Biotechnology*, *213*, 74–82. https://doi.org/10.1016/j.jbiotec.2015.01.031

Hindmarsh, A. C., Brown, P. N., Grant, K. E., Lee, S. L., Serban, R., Shumaker, D. E., & Woodward, C. S. (2005). SUNDIALS. *ACM Transactions on Mathematical Software*, *31*(3), 363–396. https://doi.org/10.1145/1089014.1089020

HiTrap™ Fibro PrismA and HiScreen™ Fibro PrismA Units Datafile, (2022). https://cdn.cytivalifesciences.com/api/public/content/digi-33339-pdf

Hjelm, H., Hjelm, K., & Sjöquist, J. (1972). Protein A from *Staphylococcus aureus*. Its isolation by affinity chromatography and its use as an immunosorbent for isolation of immunoglobulins. *FEBS Letters*, *28*(1), 73–76. https://doi.org/10.1016/0014-5793(72)80680-x

Hunt, S., Larsen, T., & Todd, R. J. (2017). Modeling preparative cation exchange chromatography of monoclonal antibodies. In *Preparative Chromatography for Separation of Proteins* (pp. 399–427). https://doi.org/10.1002/9781119031116.ch13

Ingber, L., (1993). Adaptive simulated annealing (ASA). https://github.com/ingber/adaptive-simulated-annealing

Kelley, B., Blank, G., & Lee, A. (2008). Downstream processing of monoclonal antibodies: Current practices and future opportunities. In *Process Scale Purification of Antibodies*, (pp. 1–23). https://doi.org/10.1002/9780470444894.ch1

King, J.-K., & Pinto, N. G. (1992). Short fibrous supports for preparative chromatographic separations of biomolecules. *Journal of Chromatography A*, *609*(1–2), 61–68. https://doi.org/10.1016/0021-9673(92)80149-o

Lane, V. (2018). *Computational characterization of protein A—Antibody binding*, Carnegie Mellon University. https://doi.org/10.1184/R1/7571438.V1

Lienqueo, M. E., Mahn, A., Salgado, J. C., & Shene, C. (2011). Mathematical modeling of protein chromatograms. *Chemical Engineering & Technology*, *35*(1), 46–57. https://doi.org/10.1002/ceat.201100282

Liu, H. F., Ma, J., Winter, C., & Bayer, R. (2010). Recovery and purification process development for monoclonal antibody production. *mAbs*, *2*(5), 480–499. https://doi.org/10.4161/mabs.2.5.12645

Marcus, R. K., Davis, W. C., Knippel, B. C., LaMotte, L., Hill, T. A., Perahia, D., & Jenkins, J. D. (2003). Capillary-channeled polymer fibers as stationary phases in liquid chromatography separations. *Journal of Chromatography A*, *986*(1), 17–31. https://doi.org/10.1016/s0021-9673(02)01835-6

Mollerup, J. M. (2006). Applied thermodynamics: A new frontier for biotechnology. *Fluid Phase Equilibria*, *241*(1–2), 205–215. https://doi.org/10.1016/j.fluid.2005.12.037

Mollerup, J. M. (2008). A review of the thermodynamics of protein association to ligands, protein adsorption, and adsorption isotherms. *Chemical Engineering & Technology*, *31*(6), 864–874. https://doi.org/10.1002/ceat.200800082

Montes Sanchez, F. J., Martin del Valle, E., Galan Serrano, M. A., & Cerro, R. L. (2004). Modeling of monolith-supported affinity chromatography. *Biotechnology Progress*, *20*(3), 811–817. https://doi.org/10.1021/bp034343n

Pabst, T. M., Thai, J., & Hunter, A. K. (2018). Evaluation of recent protein A stationary phase innovations for capture of biotherapeutics. *Journal of Chromatography A*, *1554*, 45–60. https://doi.org/10.1016/j.chroma.2018.03.060

Podgornik, A. (2022). Characterization of a convection-based support microstructure through a flow resistance parameter. *Journal of Separation Science*, *45*(12), 1984–1996. https://doi.org/10.1002/jssc.202100955

Ramos-de-la-Peña, A. M., González-Valdez, J., & Aguilar, O. (2019). Protein A chromatography: Challenges and progress in the purification of monoclonal antibodies. *Journal of Separation Science*, *42*(9), 1816–1827. https://doi.org/10.1002/jssc.201800963

Reck, J. M., Pabst, T. M., Hunter, A. K., Wang, X., & Carta, G. (2015). Adsorption equilibrium and kinetics of monomer–dimer monoclonal antibody mixtures on a cation exchange resin. *Journal of Chromatography A*, *1402*, 46–59. https://doi.org/10.1016/j.chroma.2015.05.007

Sandoval, G., Andrews, B. A., & Asenjo, J. A. (2012). Elution relationships to model affinity chromatography using a general rate model. *Journal of Molecular Recognition*, *25*(11), 571–579. https://doi.org/10.1002/jmr.2223

Schwan, P. (2019). *Prot-A capture model—From batch to continuous*. Presented at Chromatography Modeling Days, May 28, 2019.

Seidel-Morgenstern, A. (2020). Modeling of chromatographic processes. In *Preparative Chromatography*, (pp. 311–354). https://doi.org/10.1002/9783527816347.ch6

Shukla, A. A., Hubbard, B., Tressel, T., Guhan, S., & Low, D. (2007). Downstream processing of monoclonal antibodies—Application of platform approaches. *Journal of Chromatography B*, *848*(1), 28–39. https://doi.org/10.1016/j.jchromb.2006.09.026

Singh, A., & Pinto, N. G. (1995). Polymeric short-fiber chromatographic supports for downstream processing of biomolecules. *Reactive Polymers*, *24*(3), 229–242. https://doi.org/10.1016/0923-1137(94)00088-m

Tejeda-Mansir, A., Montesinos, R., & Guzmán, R. (2001). Mathematical analysis of frontal affinity chromatography in particle and membrane configurations. *Journal of Biochemical and Biophysical Methods*, *49*(1–3), 1–28. https://doi.org/10.1016/s0165-022x(01)00196-8

Thomas, H. C. (1944). Heterogeneous ion exchange in a flowing system. *Journal of the American Chemical Society*, *66*(10), 1664–1666. https://doi.org/10.1021/ja01238a017

Winderl, J., Hahn, T., & Hubbuch, J. (2016). A mechanistic model of ion-exchange chromatography on polymer fiber stationary phases. *Journal of Chromatography A*, *1475*, 18–30. https://doi.org/10.1016/j.chroma.2016.10.057

Yamamoto, S., Nakanishi, K., Matsuno, R., & Kamikubo, T. (1983). Ion exchange chromatography of proteins prediction of elution curves and operating conditions. I. Theoretical considerations. *Biotechnology and Bioengineering*, *25*(6), 1465–1483. https://doi.org/10.1002/bit.260250605

Yang, Y., Velayudhan, A., Ladisch, C. M., & Ladisch, M. R. (1992). Protein chromatography using a continuous stationary phase. *Journal of Chromatography A*, *598*(2), 169–180. https://doi.org/10.1016/0021-9673(92)85045-u.

SUPPORTING INFORMATION

Additional supporting information can be found online in the Supporting Information section at the end of this article.

How to cite this article: Hahn, T., Trunzer, T., Rusly, F., Zolyomi, R., Shekhawat, L. K., Malmquist, G., Hesslein, A., & Tjandra, H. (2024). Predictive scaling of fiber-based protein A capture chromatography using mechanistic modeling. *Biotechnology and Bioengineering*, *121*, 2388–2399. https://doi.org/10.1002/bit.28434